Available online at www.sciencedirect.com

SciVerse ScienceDirect

Ceramics International 39 (2013) 1495–1502

CERAMICS INTERNATIONAL

www.elsevier.com/locate/ceramint

Conductivity of Co and Ni doped lanthanum-gallate synthesized by citrate sol–gel method

Ivan Stijepovic[a,*], Azad J. Darbandi[b,c], Vladimir V. Srdic[a]

[a]*Department of Materials Engineering, Faculty of Technology, University of Novi Sad, Novi Sad, Serbia*
[b]*Structural Research Division, Technical University Darmstadt, Darmstadt, Germany*
[c]*Institute of Nanotechnology, Forschung Zentrum Karlsruhe, Karlsruhe, Germany*

Received 21 June 2012; received in revised form 20 July 2012; accepted 28 July 2012
Available online 4 August 2012

Abstract

Solid solutions of Sr and Mg doped lanthanum-gallate (LSGM) with addition of 3 and 5 at% of cobalt and nickel at the B-site in ABO_3 perovskite structure were obtained using citrate sol–gel method. The synthesized powders were calcined at 900 °C and then finally sintered at 1450 °C for only 2 h, which resulted in approximately 95% density. Impedance spectroscopy was utilized for electrical characterization in the temperature range 200–600 °C. The activation energies calculated from impedance spectra for bulk and grain boundary conductivities were decreased by the addition of transition metals (Co and Ni) and subsequently the conductivity was increased. Two different regions were clearly distinguished in the plots $\ln(\sigma T)$ vs. $10{,}000/T$ for grain boundary conductivities, indicating changes in the mechanism of charge transport with the temperature. It is concluded that addition of cobalt above 5 at% in the LSGM prepared by citrate sol–gel method does not enhance the electrolytic properties of LSGM. XRD results suggested possible coexistence of two perovskite crystalline phases in nickel doped samples. However, it is still more favorable for use in IT-SOFC applications than cobalt since it has less influence on the electrolytic domain of LSGM.

Keywords: A. Sol–gel processes; C. Ionic conductivity; D. Perovskites; E. Fuel cells

1. Introduction

Solid Oxide Fuel Cells (SOFC) are generally considered as promising devices for electrical and heat power generation. Depending on the size of stack cells a power of 1 kW up to 100 MW can be reached with fuel utilization as high as 80% at zero or low emissions. Commercially available systems are mainly based on yttria stabilized zirconia (YSZ) as electrolyte material. YSZ is a pure ionic conductor in both oxidizing and reducing atmospheres. However, the high working temperature of YSZ electrolyte is the major drawback and imposes the utilization of thin film techniques for the fabrication of thin electrolyte layers in order to reduce the working temperature below 800 °C [1,2]. Nevertheless, this temperature range is still too high for the use of cost effective stack components (e.g. steel as current collector) and demands a long start-up time. Several materials such as doped ceria (CeO_2), bismuth-oxide (Bi_2O_3) and lanthanum-gallate ($LaGaO_3$) have been proposed to replace YSZ [1,3,4]. Doped ceria and bismuth oxide have higher ionic conductivities than YSZ but mixed conductivity in reducing atmospheres [3,4]. Sr and Mg doped $LaGaO_3$ (LSGM) are reported in literature as pure ionic conductors in a wide range of oxygen partial pressures and substantially higher conductivity than YSZ below 800 °C [3–9].

Ishihara et al. [3] reported a high ionic conductivity of 0.31 S cm^{-1} at 1000 °C for the LSGM and since then various studies have been made on synthesis and characterization of this material system [5,10–12]. Alternative synthesis such as co-precipitation, combustion synthesis, Pechini method and plasma spraying have been also reported [10,13–26]. However, all of these methods suffer from similar problems such as long calcination and sintering times, presence of secondary phases and low

*Corresponding author. Tel.: +381214853750; fax: +38121450413.
E-mail address: ivan@tf.uns.ac.rs (I. Stijepovic).

0272-8842/$ - see front matter © 2012 Elsevier Ltd and Techna Group S.r.l. All rights reserved.
http://dx.doi.org/10.1016/j.ceramint.2012.07.096

density (93–95% of the theoretical density). In our previous work [27] we reported a modified Pechini synthesis of LSGM called citrate sol–gel method [28]. The citrate sol–gel method offers substantially better control of stoichiometry, especially in multi component material systems, as there are no washing or filtering steps. Powders prepared by citrate sol–gel method can be further processed for the fabrication of thin electrolytes (<50 μm) [29].

Substitutional doping of B-site with transition metals (Co, Ni, and Fe) can further improve the ionic conductivity of LSGM without significant decrease in oxygen transference number [30–38]. Modified compositions of LSGM have been utilized by Kansai Electric Power Co., Inc. (KEPCO) and Mitsubishi Materials Corporation (MMC) for the fabrication of IT-SOFC stacks of 1–10 kW based on natural gas as a fuel [39,40]. They showed that Co doped LSGM could be successfully applied as an electrolyte for SOFC working at temperatures below 800 °C and still providing high efficiency and enabling long time stability.

It has been considered that the electrolyte material should have an ionic conductivity of about 0.01 S cm^{-1} at temperatures below 800 °C in order to be used in IT-SOFC. With LSGM this demand is already fulfilled at ~600 °C [5]. The highest ionic conductivities were reported for the $La_{1-x}Sr_xGa_{1-y}Mg_yO_{3-\delta}$ ($0.1 \le x,\ y \le 0.2$) material system. Higher ionic conductivity can be achieved by increasing the doping level which in turn increases the number of oxygen vacancies. Nevertheless, the solid solubility of Sr in Mg in the perovskite structure of $LaGaO_3$ is limited and higher doping levels lead to the formation of secondary phases which in turn affects the conductivity. There are contradictory reports on solubility limits of Sr and Mg, which can be explained by the use of different synthesis routes and preparation conditions. In our earlier studies, high level doped single phase $La_{0.85}Sr_{0.15}Ga_{0.8}Mg_{0.2}O_{3-\delta}$ with high ionic conductivity at 600 °C ($\sigma = 0.01$ S cm^{-1}) was achieved by the citrate sol–gel method [27]. In this work, the effect of partial substitution (3 and 5 at%) of Mg by Co or Ni in $La_{0.85}Sr_{0.15}Ga_{0.8}Mg_{0.2}O_{3-\delta}$ will be discussed.

2. Experimental

Stoichiometric amounts of the nitrates $La(NO_3)_3 \cdot 6H_2O$ (Riedel-de Haen), $Ga(NO_3)_3 \cdot xH_2O$ (Merck), $Sr(NO_3)_2$ (Fluka), $Mg(NO_3)_2 \cdot 6H_2O$ (Merck), $Co(NO_3)_2 \cdot 6H_2O$ (Merck), and $Ni(NO_3)_2$ (Fluka), were dissolved in distilled water to form solutions with a total cation concentration of 0.2 M. The level of hydration in gallium nitrate was determined experimentally by thermogravimetric analysis (BAHR Thermoanalyse STA503). Citric acid was added with molar ratio of 2:1 to the total cations in the solution. The solution was stirred for 1 h at room temperature, followed by 1 h at 80 °C. The solution was then evaporated until a dark yellow resin formed. After drying at 120 °C for 12 h the obtained yellow foam was ground and subsequently calcined. The calcination was performed with a heating rate of 1 °C/min below 270 °C followed by 5 °C/min (270–900 °C), and kept at 900 °C for 1 h.

Table 1
Chemical composition, notation of the samples and results of image analysis with Gwyddion 2.25.

Sample name	Chemical composition	Pore fraction (%)	Grains fraction (%)
L85G80	$La_{0.85}Sr_{0.15}Ga_{0.80}Mg_{0.2}O_{2.825}$	–	–
L85G80C3	$La_{0.85}Sr_{0.15}Ga_{0.80}Mg_{0.17}Co_{0.03}O_{2.825}$	4.3	95.7
L85G80C5	$La_{0.85}Sr_{0.15}Ga_{0.80}Mg_{0.15}Co_{0.05}O_{2.825}$	3	97
L85G80N3	$La_{0.85}Sr_{0.15}Ga_{0.80}Mg_{0.17}Ni_{0.03}O_{2.825}$	2.4	97.6
L85G80N5	$La_{0.85}Sr_{0.15}Ga_{0.80}Mg_{0.15}Ni_{0.05}O_{2.825}$	5.7	94.3

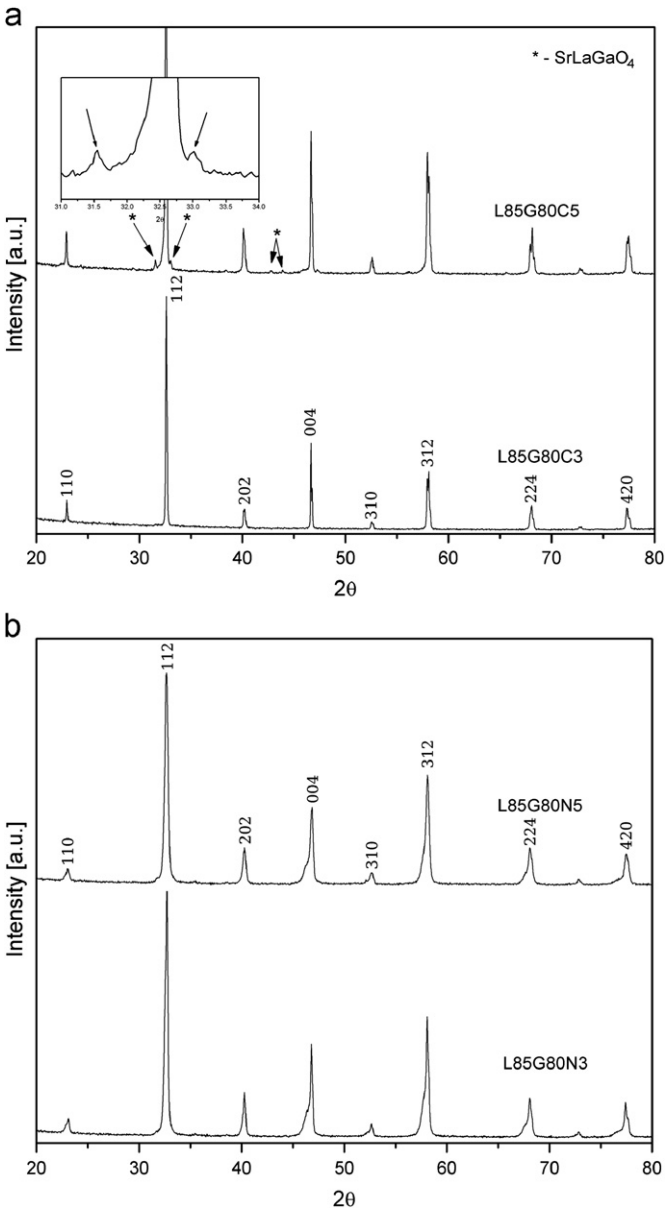

Fig. 1. XRD results of the sintered samples: (a) with cobalt and (b) with nickel.

Calcined powders were uniaxially pressed at a pressure of 625 MPa in a steel die to form pellets and then sintered. The temperature regime of sintering had several stages. The heating rate of 5 °C/min was used at first with 1 h dwell at 500 °C, followed by heating at the rate of 10 °C/min up to 1450 °C with 2 h hold at this temperature. The temperature was then decreased by 10 °C/min to room temperature. Notation of samples is given in Table 1.

Structural analysis was performed by X-ray diffraction method (PANalytical X'Pert PRO) using Cu–Kα radiation and wavelength of 0.15406 nm with a step of 0.03°/s. Scanning electron microscopy (SEM, JEOL JSM 6460LV) was used to analyze the microstructure and to determine the density of the sintered samples. Samples were ground and polished and thermally etched at 1300 °C for 30 min. ImageJ 1.44p [42] and Gwyddion 2.25 [43] software were used for SEM image analysis. Density was also measured by the Archimedes method in distilled water. Conductivity measurements were performed by means of impedance spectroscopy (Solartron 1260 Impedance Analyzer) in the temperature range 200–600 °C and frequency range 0.05–1 MHz with a perturbation voltage

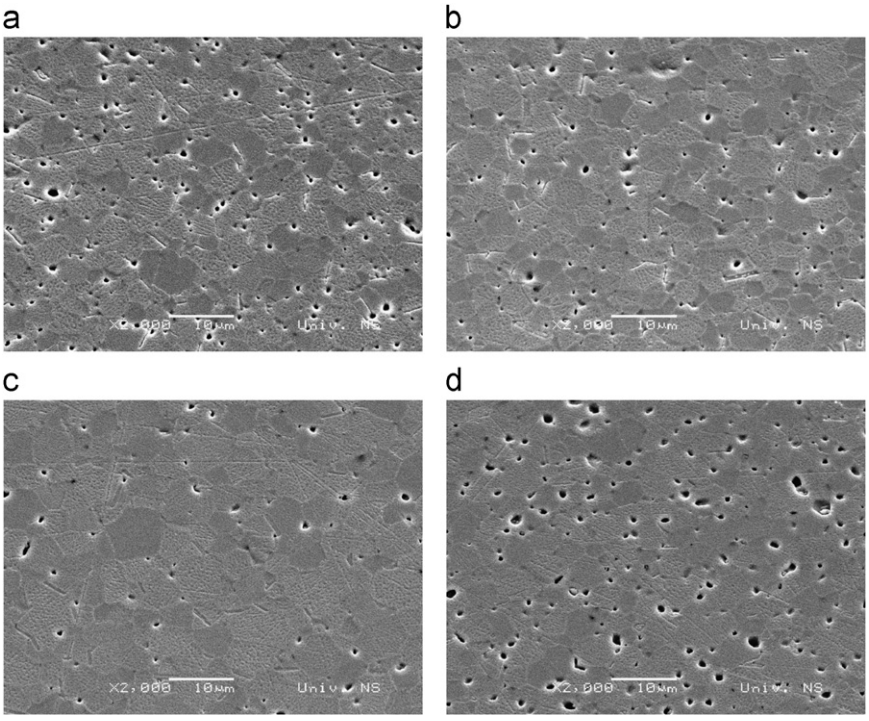

Fig. 2. SEM images of the sintered samples at x2000 magnification: (a) L85G80C3; (b) L85G80C5; (c) L85G80N3; and (d) L85G80N5.

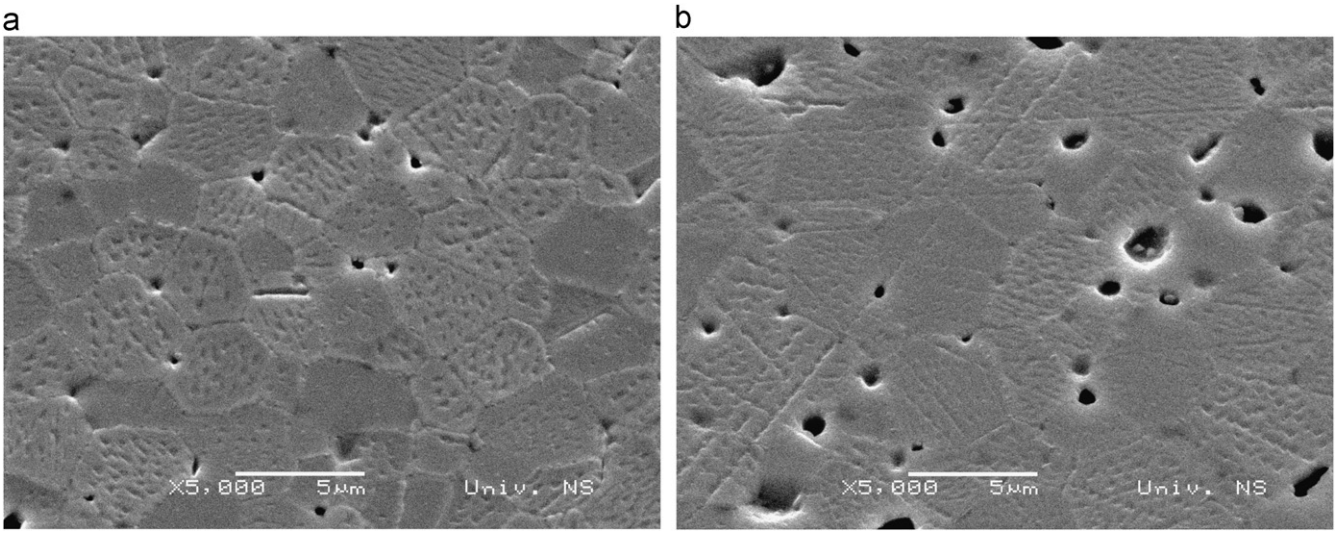

Fig. 3. SEM images for the sintered samples with 5 at% of transition metal at x5000 magnification: (a) L85G80C5 and (b) L85G80N5.

of 30 mV. As current collectors 50 nm thin layers of gold were sputtered on both sides of the pellets. A frequently suggested equivalent circuit [44] was used in order to fit the impedance spectra and the conductivity values were extracted from the ZView2 software.

3. Results and discussion

XRD results of sintered samples are shown in Fig. 1. Solid solutions with cobalt could be identified as orthorhombic perovskite phase since there is obvious peak splitting in reflections 202, 312, 224 and 420, which are characteristic of this crystal structure (Fig. 1a). Additionally, by substitution of Mg by 5 at% cobalt, there is a small amount of secondary phase identified as tetragonal $SrLaGaO_4$ (JCPDS 24-1208). This could be a consequence of the decrease in Sr solubility in the solid solution since it is highly dependent on the amount of Mg present [41]. As magnesium content decreased from 20 to 15 at% in L85G80C5, Sr solubility dropped from its initial value of 15 at% to lower values and excess of strontium formed in the afore-mentioned secondary phase.

In the case of nickel doping (Fig. 1b), there is no peak splitting but the shape of the peaks is not symmetrical, which could indicate the presence of two phases. Similar behavior is reported for LSGM ceramics by Shkerin et al. [45] and they assigned it to the change in chemical composition only at the surface of the sample. Rozumek

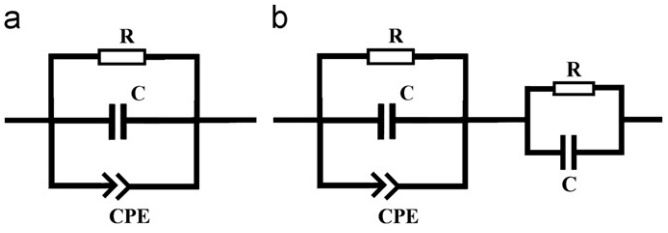

Fig. 5. Equivalent circuits used for fitting IS spectra: (a) parallel R–C–CPE circuit and (b) parallel R–C–CPE circuit in series with parallel R–C circuit.

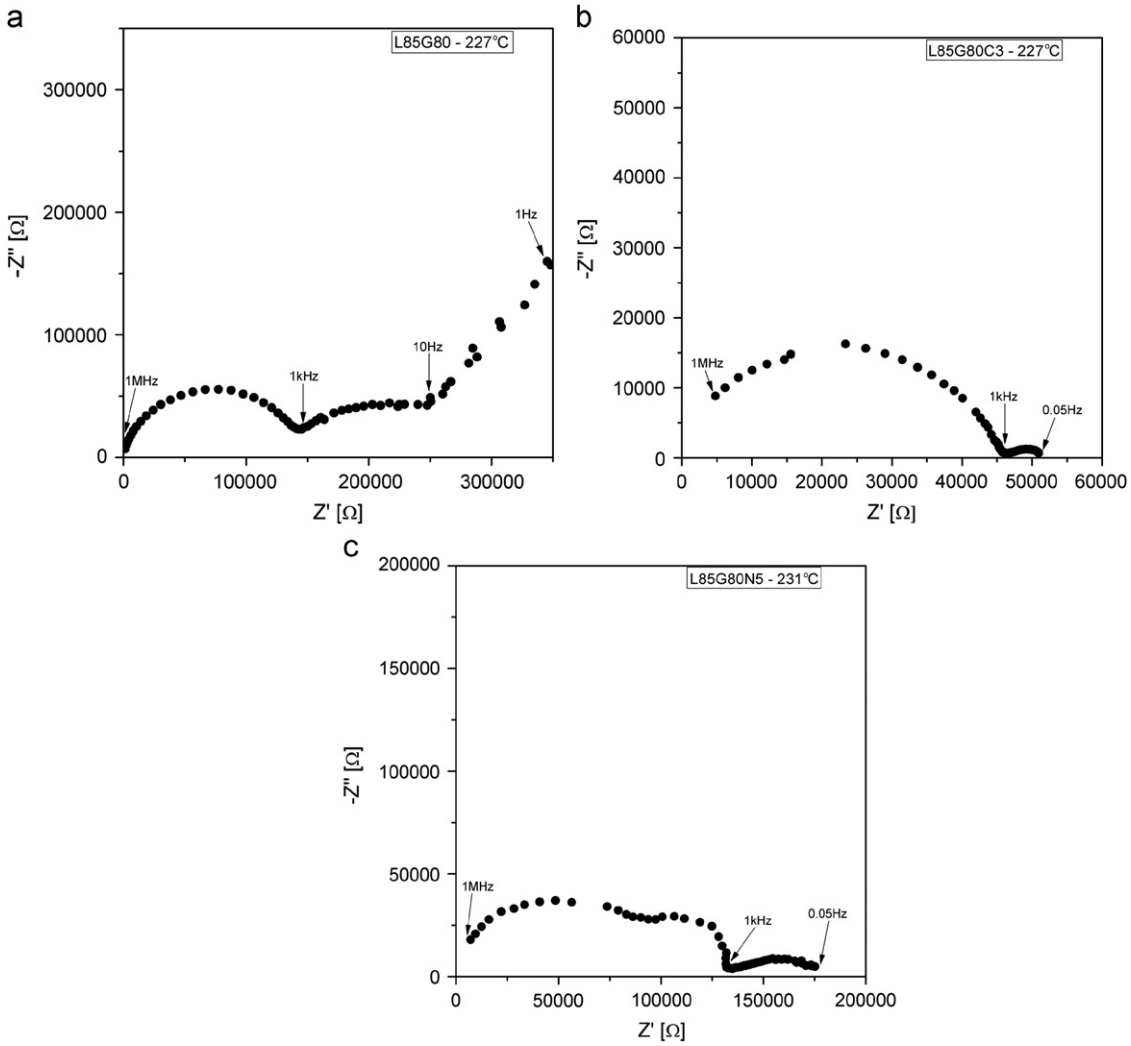

Fig. 4. IS spectra for three different samples: (a) L85G80; (b) L85G80C3; and (c) L85G80N5.

et al. [46] reported that lanthanum-gallate perovskite phases containing 15–20 at% of Sr and 15–20 at% of Mg are metastable in their nature and exist in orthorhombic, rhombohedral and cubic forms depending on the composition and sintering temperatures and time. Considering the very short sintering time used in this work (only 2 h) and the influence of Ni addition, it is possible that two different lanthanum-gallate crystal structures are present and coexist in the bulk ceramics.

According to SEM images (Fig. 2), samples were not fully dense after sintering at 1450 °C for 2 h. This indicates that the sintering time should be prolonged in order to obtain higher density. However, image analysis at several different magnifications showed that pore fraction is from 2 to 6% of the image (Table 1). Also, it should be noted that the sample with 3 at% of nickel had the highest density after sintering, which was 97.4% of the theoretical density as measured by Archimedes' method. This result is in good agreement with the value of 97.6% of the grain fraction given in Table 1. There are also some structural defects along grain boundaries visible at higher magnification, shown in Fig. 3. However, it is not possible to ascribe them to the presence of a secondary phase. More likely, they are the consequence of the increased roughness induced by thermal etching.

Impedance spectroscopy has been used for the electrical characterization of samples in the temperature range 200–600 °C (Fig. 4). Different equivalent circuits have been applied in order to fit the experimental data (Fig. 5). It should be noted that the given circuits were not used to fit the whole spectra but rather separate regions corresponding to bulk and grain boundary responses. The first equivalent circuit (Fig. 5a) gave the best fit for sample L85G80 and for the samples with cobalt. There was no need for additional elements (Fig. 5b) as suggested by Abram et al. [44], neither for bulk nor grain boundary response. However, in the case of nickel doping, a new semicircle component appeared in the bulk region (Fig. 4c) and the equivalent circuit shown in Fig. 5b resulted in the best fit for bulk response. This could be explained by the presence of another perovskite crystal

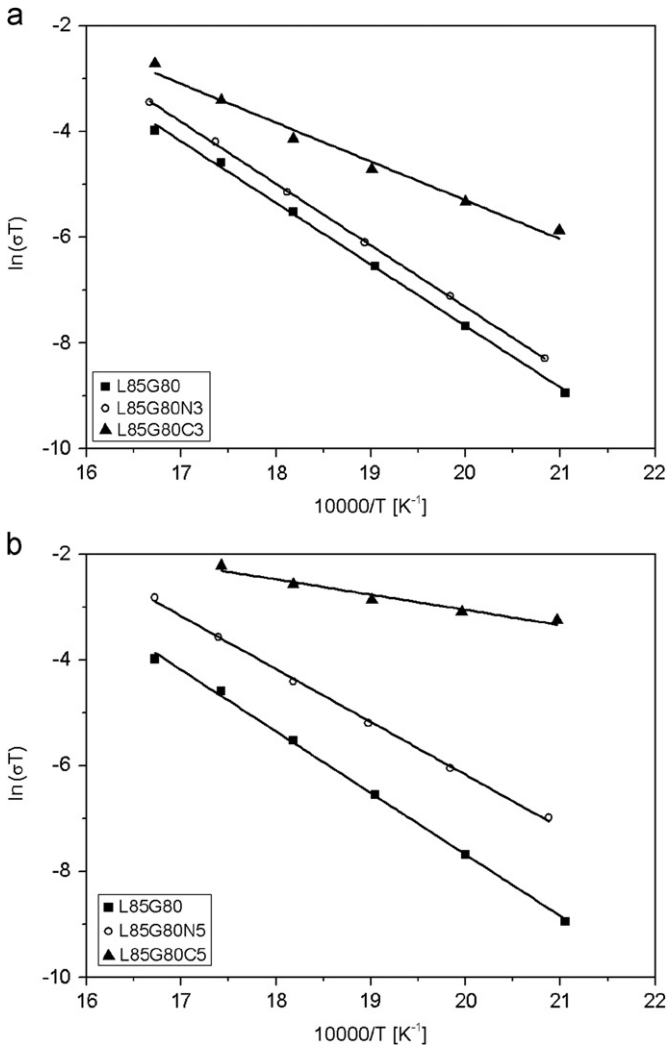

Fig. 6. Bulk conductivities for samples with different amounts of transition metals: (a) 3 at% and (b) 5 at%.

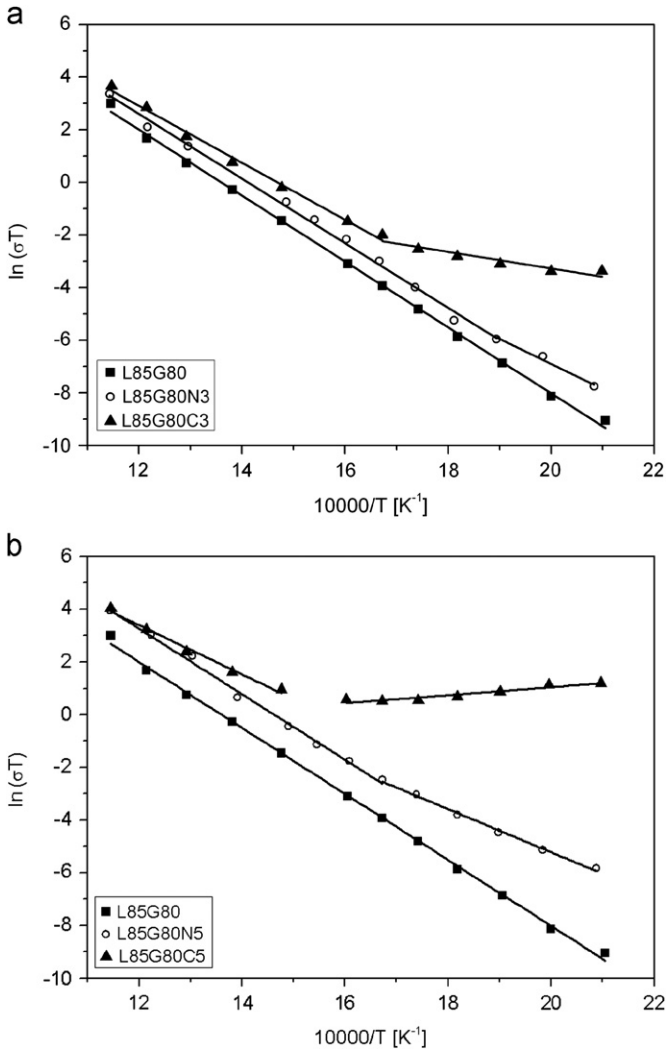

Fig. 7. Grain boundary conductivities for samples with different amounts of transition metals: (a) 3 at% and (b) 5 at%.

Table 2
Activation energies for bulk and grain boundary conductivities in electron volts.

Sample name	E_{bulk} (eV)	E_{gb1} (eV)	E_{gb2} (eV)
L85G80	1.004	1.079	
L85G80C3	0.633	0.211	0.932
L85G80C5	0.249	−0.130	0.806
L85G80N3	1.006	0.819	1.058
L85G80N5	0.863	0.706	1.073

phase in the bulk of the material which is indicated by the XRD results as well. It should be noted that this behavior is only visible in the bulk part of the impedance spectra of the LSGMN samples and it could not be observed in the grain boundary region (low frequency part in Fig. 4c).

It can be seen from Figs. 6 and 7 that doping with Co and Ni increased both the bulk and grain boundary conductivities, as expected. There is no bulk response visible above 325 °C and the fitting was possible only below this temperature giving a single slope in the $\ln(\sigma_b T)$ vs. $10{,}000/T$ plot. Activation energies of the bulk conductivities for samples L85G80 and L85G80N3 (Table 2) are almost the same as reported by Kurumada et al. [12]. However, the activation energy for the sample with 5 at% of Ni is somewhat lower than reported, while the samples with cobalt show significantly lower values.

On the other hand, the grain boundary semicircle could be identified throughout the temperature range. The addition of cobalt and nickel in L85G80 had a significant impact on the grain boundary conductivity and changed the activation energy drastically (Table 2). There are two different activation energy values at two temperature ranges in $\ln(\sigma_{gb}T)$ vs. $10{,}000/T$ plots, both at 3 and 5 at% of the dopants. Similar results were reported for the total conductivity by Huang et al. [33] for the cobalt and nickel doped LSGM prepared by the solid state reaction. It is well known that doping with transition metals somewhat increases the hole conductivity, especially at lower temperatures and higher oxygen partial pressures, and it has been suggested that the optimal content of Co for solid state route is about 8.5 at% for IT-SOFC [30,31,47]. However, the addition of only 5 at% of cobalt in our study led to metallic-like behavior of the samples with negative value of E_a below 350 °C for grain boundary conductivity (Table 2). This could indicate the formation of cobalt-rich regions along the grain boundaries and its oxidation from 2+ to 3+. Higher level of Co doping could shift this transition temperature to higher values and would significantly reduce the electrolytic region of LSGMC. However, L85G80C5 could still be used as the electrolyte for IT-SOFC since above 350 °C ionic conductivity is still the dominant conduction mechanism. Therefore, in the citrate sol–gel synthesis which was used, 5 at% of cobalt is probably the highest content possible for LSGM ceramics with practical applications.

In the nickel doped samples (L85G80N3 and L85G80N5), there are also two slopes in the grain boundary conductivity plots (Fig. 7) but the decrease in E_a is not as pronounced as with cobalt and at higher temperatures it is quite close to the literature data [12]. Nickel also increased the conductivity of the L85G80 but without such significant influence on the hole conductivity which is very important for electrolyte application. From the point of view of electrolytic domains, this could indicate that doping with Ni in citrate method is more favorable than with Co which agrees well with literature reports.

4. Conclusions

The citrate sol–gel method has been used to synthesize solid solutions of $La_{0.85}Sr_{0.15}Ga_{0.8}Mg_{0.2}O_{3-\delta}$ with 3 and 5 at% Mg substitution by cobalt and nickel. Phase composition was influenced by the amount and type of the transition metal. With addition of transition metals both bulk and grain boundary conductivities were increased. In the case of nickel doping, XRD results suggested the coexistence of two different lanthanum-gallate perovskite crystal phases. Impedance spectroscopy of nickel doped samples showed the appearance of the second semicircle in the bulk response and two new elements were added to the equivalent circuit in order to fit the bulk region in those samples. Activation energies for conductivities were significantly decreased and even metallic-like behavior was observed for the sample with 5 at% of Co at lower temperatures. It is concluded that this is the highest content of Co addition in the $La_{0.85}Sr_{0.15}Ga_{0.8}Mg_{0.2}O_{3-\delta}$ electrolyte material which is possible to obtain with citrate sol–gel method, keeping in mind its IT-SOFC application. On the other hand, nickel increased conductivity but it showed milder impact on hole conductivity in comparison with cobalt.

Acknowledgments

This work was supported by the Serbian Ministry of Education and Science, under Project no. III45021, and COST 539 Project ELENA.

References

[1] N.Q. Minh, Solid oxide fuel cell technology—features and applications, Solid State Ionics 174 (2004) 271–277.
[2] M.C. Williams, J.P. Strakey, W.A. Surdoval, L.C. Wilson, Solid oxide fuel cell technology development in the US, Solid State Ionics 177 (2006) 2039–2044.
[3] T. Ishihara, H. Matsuda, Y. Takita, Doped $LaGaO_3$ perovskite type oxide as a new oxide ionic conductor, Journal of the American Chemical Society 116 (1994) 3801–3803.
[4] T. Ishihara, H. Matsuda, Y. Takita, Effects of rare earth cations doped for La site on the oxide ionic conductivity of $LaGaO_3$-based perovskite type oxide, Solid State Ionics 79 (1995) 147–151.
[5] K. Huang, R.S. Tichy, J.B. Goodenough, Superior perovskite oxide–ion conductor; strontium- and magnesium-doped $LaGaO_3$:I, phase

relationships and electrical properties, Journal of the American Ceramic Society 81 (10) (1998) 2565–2575.
[6] K. Huang, R.S. Tichy, J.B. Goodenough, Superior perovskite oxide–ion conductor; strontium- and magnesium-doped $LaGaO_3$: II, ac impedance spectroscopy, Journal of the American Ceramic Society 81 (10) (1998) 2576–2580.
[7] K. Huang, J.B. Goodenough, A solid oxide fuel cell based on Sr- and Mg-doped $LaGaO_3$ electrolyte: the role of rare-earth oxide buffer, Journal of Alloys and Compounds 303–304 (2000) 454–464.
[8] W. Gong, S. Gopalan, U.B. Pal, Performance of intermediate temperature (600–800 °C) solid oxide fuel cell based on Sr and Mg doped lanthanum-gallate electrolyte, Journal of Power Sources 160 (2006) 305–315.
[9] N.M. Sammes, Y. Du, Fabrication and characterization of tubular solid oxide fuel cells, International Journal of Applied Ceramic Technology 4 (2) (2007) 89–102.
[10] E. Djurado, M. Labeau, Second phases in doped lanthanum gallate perovskites, Journal of the European Ceramic Society 18 (1998) 1397–1404.
[11] M. Rozumek, P. Majewski, L. Sauter, F. Aldinger, Homogeneity region of strontium- and magnesium-containing $LaGaO_3$ at temperatures between 1100° and 1500 °C in air, Journal of the American Ceramic Society 86 (11) (2003) 1940–1946.
[12] M. Kurumada, H. Hara, F. Munakata, E. Iguchi, Electric conductions in $La_{0.9}Sr_{0.1}GaO_{3-\delta}$ and $La_{0.9}Sr_{0.1}Ga_{0.9}Mg_{0.1}O_{3-\delta}$, Solid State Ionics 176 (2005) 245–251.
[13] P. Majewski, M. Rozumek, C.A. Tas, F. Aldinger, Processing of $(La,Sr)(Ga,Mg)O_3$ solid electrolyte, Journal of Electroceramics 8 (2002) 65–73.
[14] A. Tarancón, G. Dezanneau, J. Arbiol, F. Peiró, J.R. Morante, Synthesis of nanocrystalline materials for SOFC applications by acrylamide polymerisation, Journal of Power Sources 118 (2003) 256–264.
[15] R. Pelosato, I. Natali Sora, V. Ferrari, G. Dotelli, C.M. Mari, Preparation and characterisation of supported $La_{0.83}\cdot Sr_{0.17}$ $Ga_{0.83}$ $Mg_{0.17}$ $O_{2.83}$ thick films for application in IT-SOFCs, Solid State Ionics 175 (2004) 87–92.
[16] M. Shi, N. Liu, Y. Xu, Y. Yuan, P. Majewski, F. Aldinger, Synthesis and characterization of Sr- and Mg-doped $LaGaO_3$ by using glycine–nitrate combustion method, Journal of Alloys and Compounds 425 (2006) 348–352.
[17] M. Ohnuki, K. Fujimoto, S. Ito, Preparation of high-density $La_{0.90}Sr_{0.10}Ga_{1-y}Mg_yO_{-\delta}$ (y=0.20 and 0.30) oxide ionic conductors using HIP, Solid State Ionics 177 (2006) 1729–1732.
[18] C. Oncel, B. Ozkaya, M.A. Gulgun, X-ray single phase LSGM at 1350 °C, Journal of the European Ceramic Society 27 (2007) 599–604.
[19] H. Ishikawa, M. Enoki, T. Ishihara, T. Akiyama, Self-propagating high-temperature synthesis of $La(Sr)Ga(Mg)O_{3-\delta}$ for electrolyte of solid oxide fuel cells, Journal of Alloys and Compounds 430 (2007) 246–251.
[20] B. Liu, Y. Zhang, $La_{0.9}Sr_{0.1}Ga_{0.8}Mg_{0.2}O_{3-\delta}$ sintered by spark plasma sintering (SPS) for intermediate temperature SOFC electrolyte, Journal of Alloys and Compounds 458 (2008) 383–389.
[21] T.Y. Chen, K.Z. Fung, Synthesis of and densification of oxygen-conducting $La_{0.8}Sr_{0.2}Ga_{0.8}Mg_{0.2}O_{2.8}$ nano powder prepared from a low temperature hydrothermal urea precipitation process, Journal of the European Ceramic Society 28 (2008) 803–810.
[22] M. Kumar, S. Srikanth, B. Ravikumar, T.C. Alex, S.K. Das, Synthesis of pure and Sr-doped $LaGaO_3$, $LaFeO_3$ and $LaCoO_3$ and Sr,Mg-doped $LaGaO_3$ for ITSOFC application using different wet chemical routes, Materials Chemistry and Physics 113 (2009) 803–815.
[23] M. Shi, Y. Xu, A. Liu, N. Liu, C. Wanga, P. Majewski, F. Aldinger, Synthesis and characterization of Sr- and Mg-doped Lanthanum gallate electrolyte materials prepared via the Pechini method, Materials Chemistry and Physics 114 (2009) 43–46.
[24] R. Pelosato, C. Cristiani, G. Dotelli, S. Latorrata, R. Ruffo, Luca Zampori, Co-precipitation in aqueous medium of $La_{0.8}Sr_{0.2}Ga_{0.8}Mg_{0.2}O_{3-\delta}$ via inorganic precursors, Journal of Power Sources 195 (2010) 8116–8123.
[25] C.S. Hwanga, C.H. Tsai, J.F. Yu, C.L. Chang, J.M. Lin, Y.H. Shiu, S.W. Cheng, High performance metal-supported intermediate temperature solid oxide fuel cells fabricated by atmospheric plasma spraying, Journal of Power Sources 196 (2011) 1932–1939.
[26] S.B. Ha, Y.H. Cho, H.I. Ji, J.H. Lee, Y.C. Kang, J.H. Lee, Low-temperature sintering and electrical properties of strontium- and magnesium-doped lanthanum gallate with V_2O_5 additive, Journal of Power Sources 196 (2011) 2971–2978.
[27] I. Stijepovic, A.J. Darbandi, V.V. Srdic, Conductivity of doped $LaGaO_3$ prepared by citrate sol–gel process, Journal of Optoelectronics and Advanced Materials 12 (5) (2010) 1098–1104.
[28] R. Polini, A. Pamio, E. Traversa, Effect of synthetic route on sintering behaviour, phase purity and conductivity of Sr- and Mg-doped $LaGaO_3$ perovskites, Journal of the European Ceramic Society 24 (2004) 1365–1370.
[29] W. Wang, Z. Yang, H. Wang, G. Ma, W. Gao, Z. Zhou, Desirable performance of intermediate-temperature solid oxide fuel cell with an anode-supported $La_{0.9}Sr_{0.1}Ga_{0.8}Mg_{0.2}O_{3-\delta}$ electrolyte membrane, Journal of Power Sources 196 (2011) 3539–3543.
[30] T. Ishihara, T. Akbay, H. Furutani, Y. Takita, Improved oxide ion conductivity of Co doped $La_{0.8}Sr_{0.2}Ga_{0.8}Mg_{0.2}O_3$ perovskite type oxide, Solid State Ionics 113–115 (1998) 585–591.
[31] T. Ishihara, H. Furutani, M. Honda, T. Yamada, T. Shibayama, T. Akbay, N. Sakai, H. Yokokawa, Y. Takita, Improved oxide ion conductivity in $La_{0.8}Sr_{0.2}Ga_{0.8}Mg_{0.2}O_3$ by doping Co, Chemistry of Materials 11 (1999) 2081–2088.
[32] H. Ullmann, N. Trofimenko, A. Naoumidis, D. Stöver, Ionic/electronic mixed conduction relations in perovskite-type oxides by defect structure, Journal of the European Ceramic Society 19 (1999) 791–796.
[33] K. Huang, J. Wan, J.B. Goodenough, Oxide–ion conducting ceramics for solid oxide fuel cells, Journal of Materials Science 36 (2001) 1093–1098.
[34] V.V. Kharton, F.M.B. Marques, A. Atkinson, Transport properties of solid oxide electrolyte ceramics: a brief review, Solid State Ionics 174 (2004) 135–149.
[35] T. Ishihara, S. Ishikawa, K. Hosoi, H. Nishiguchi, Y. Takita, Oxide ionic and electronic conduction in Ni-doped $LaGaO_3$-based oxide, Solid State Ionics 175 (2004) 319–322.
[36] T. Ishihara, J. Tabuchi, S. Ishikawa, J. Yan, M. Enoki, H. Matsumoto, Recent progress in $LaGaO_3$ based solid electrolyte for intermediate temperature SOFCs, Solid State Ionics 177 (2006) 1949–1953.
[37] M. Enoki, J. Yan, H. Matsumoto, T. Ishihara, High oxide ion conductivity in Fe and Mg doped $LaGaO_3$ as the electrolyte of solid oxide fuel cells, Solid State Ionics 177 (2006) 2053–2057.
[38] A. Nobuta, F.F. Hsieh, T.H. Shin, S. Hosokai, S. Yamamoto, N. Okinaka, T. Ishihara, T. Akiyama, Self-propagating high-temperature synthesis of $La(Sr)Ga(Mg,Fe)O_{3-\delta}$ with planetary ball–mill treatment for solid oxide fuel cell electrolytes, Journal of Alloys and Compounds. 509 (2011) 8387–8391.
[39] F. Nishiwaki, T. Inagaki, J. Kano, J. Akikusa, N. Murakami, K. Hosoi, Development of disc-type intermediate-temperature solid oxide fuel cell, Journal of Power Sources 157 (2006) 809–815.
[40] T. Inagaki, F. Nishiwaki, S. Yamasaki, T. Akbay, K. Hosoi, Intermediate temperature solid oxide fuel cell based on lanthanum gallate electrolyte, Journal of Power Sources 181 (2008) 274–280.
[41] V.P. Gorelov, D.J. Bronin, Ju.V. Sokolova, H. Nafe, F. Aldinger, The effect of doping and processing conditions on properties of $La_{1-x}Sr_xGa_{1-y}Mg_yO_{3-\alpha}$, Journal of the European Ceramic Society 21 (2001) 2311–2317.
[42] 〈http://imagej.nih.govs/ij/index.html〉.
[43] 〈http://gwyddion.net/〉.

[44] E.J. Abram, D.C. Sinclair, A.R. West, A strategy for analysis and modelling of impedance spectroscopy data of electroceramics: doped lanthanum gallate, Journal of Electroceramics 10 (2003) 165–177.

[45] S.N. Shkerin, D.I. Bronin, S.A. Kovyazina, V.P. Gorelov, A.V. Kuz'min, Z.S. Martem'yanova, S.M. Beresnev, Structure and electric conductivity of (La,Sr)(Ga,Mg)$O_{3-\alpha}$ solid electrolyte, Journal of Structural Chemistry 44 (2) (2003) 216–221.

[46] M. Rozumek, P. Majewski, F. Aldinger, Metastable crystal structure of strontium- and magnesium-substituted $LaGaO_3$, Journal of the American Ceramic Society 87 (4) (2004) 656–661.

[47] J. Xue, Y. Shen, Q. Zhou, T. He, Y. Han, Combustion synthesis and properties of highly phase-pure perovskite electrolyte Co-doped $La_{0.9}Sr_{0.1}Ga_{0.8}Mg_{0.2}O_{2.85}$ for IT-SOFCs, International Journal of Hydrogen Energy 35 (2010) 294–300.